Supplementary Information for

Oxime-modified hierarchical self-assembly polyimide microspheres for high-efficient uranium recovery from wastewater

Lien Zhu [a], Chunhong Zhang [a, b*], Fuqiu Ma [b, c], Changlong Bi [a], Ruiqi Zhu [a], Feifan Qin [a], Lijia Liu [a, b*], Jianwei Bai [a*], Hongxing Dong [a] and Toshifumi Satoh [d]

[a] Key Laboratory of Superlight Materials and Surface Technology of Ministry of Education, College of Materials Science and Chemical Engineering, Harbin Engineering University, Harbin, 150001, P. R. China.

[b] Yantai Research Institute and Graduate School of Harbin Engineering University, Yantai, 264006, P.R. China.

[c] College of Nuclear Science and Technology, Harbin Engineering University, Harbin, 150001, P. R. China.

[d] Faculty of Engineering, Hokkaido University, Sapporo, 060-8628, Japan

* Corresponding authors.

E-mail addresses: zhangchunhong97@163.com (C. Zhang) liulijia@hrbeu.edu.cn (L. liu) baijw559@163.com (J. Bai).

Tel: +86-451-82568191 (C. Zhang)

S1 Batch adsorption studies

In the batch adsorption studies, the effects of pH, contact time, initial uranium concentration, and temperature on the adsorption capacity were studied. Briefly, 10 mg HSPI-O was dispersed into a flask loaded with 50 mL uranium-bearing solution (10 mg L^{-1}-300 mg L^{-1}), which was kept in a thermostatic shaker bath for *t* hours at the temperature of *T*. The 0.1 M Na_2CO_3 and HNO_3 were used to adjust the pH of the uranium-bearing solution. After the adsorption process was completed, the adsorbent was centrifuged and collected after vacuum drying overnight, which was labeled as HSPI-O-U. The detailed methods were as followed:

Influences of pH:

Since the general pH range of uranium-containing wastewater is 5-7, this study selects a wider pH range (3-9) to study the influence of pH on the adsorption capacities of the adsorbent. Seven 50 mL 100 mg L^{-1} uranium-bearing solution were configured in seven flasks. The 0.1 M Na_2CO_3 and HNO_3 were used to adjust the pH of the uranium-bearing solution to 3, 4, 5, 6, 7, 8, and 9. 10 mg HSPI-O was dispersed into each flask, which was kept in a thermostatic shaker bath for 16 h at 298 K. After adsorption equilibrium, the equilibrium uranium concentrations were detected and the adsorption capacities were calculated. The HSPI was tested using the same method

Effect of contact time:

In order to explore the effect of adsorption time on adsorption capacities, the adsorption capacities at different time points (0.2 h, 0.5 h, 1.0 h, 1.5h, 2.0 h, 3.0

h, 4.0 h, 5.0 h, 6.0 h, 10.0 h, 16.0 h) were studied. Eleven flasks were used to configure 50 mL 100 mg L^{-1} uranium-bearing solution. The 0.1 M Na_2CO_3 and HNO_3 were used to adjust the pH of the uranium-bearing solution to 6. 10 mg HSPI-O was dispersed into each flask, which was kept in a thermostatic shaker bath for 0.2 h, 0.5 h, 1.0 h, 1.5 h, 2.0 h, 3.0 h, 4.0 h, 5.0 h, 6.0 h, 10.0 h and 16.0 h at 298 K. The residual concentrations of uranium were detected and the adsorption capacities were calculated. When the pH is 5, the same method was used to test the adsorption capacities of HSPI-O.

Effect of initial uranium concentration:

In order to explore the influence of the initial uranium concentration on the adsorption capacities of the adsorbent, a variety of concentrations of uranium solution (10 mg L^{-1}, 25 mg L^{-1}, 45 mg L^{-1}, 85 mg L^{-1}, 170 mg L^{-1}, 250 mg L^{-1}, 300 mg L^{-1}) were selected to explore its maximum adsorption capacity. Seven 50 mL uranium-bearing solution with different uranium concentration were configured in seven flasks. The 0.1 M Na_2CO_3 and HNO_3 were used to adjust the pH of the uranium-bearing solution to 6. 10 mg HSPI-O was dispersed into each flask, which was kept in a thermostatic shaker bath for 16 h at 298 K. After the adsorption, the equilibrium uranium concentrations were detected and the adsorption capacities were calculated.

Effect of temperature

Taking into account the actual use temperature of the adsorbent and referring to related literature, four temperatures (298 K, 303 K, 308 K, 313 K) were selected as the test conditions. Four 50 mL 100 mg L^{-1} uranium-bearing solution were configured in four flasks. The 0.1 M Na_2CO_3 and HNO_3 were used to adjust

the pH of the uranium-bearing solutions to 6. 10 mg HSPI-O was dispersed into each flask, which was kept in a thermostatic shaker bath for 16 h at different temperature. After the adsorption, the equilibrium uranium concentrations were detected and the adsorption capacities were calculated.

S2 Selective adsorption and simulated nuclear wastewater adsorption test

Selective adsorption :

To explore HSPI-O selective adsorption performance, seven interfering ions (K^+,Ca^{2+},Na^+,Mg^{2+},Cs^+,Sr^{2+},Zn^{2+}) which often appear in uranium-containing wastewater were selected for selective adsorption testing. The experiment process was similar to the batch adsorption studies. Seven 50mL uranium-bearing solution with different interfering ions were configured in seven flasks. The concentration of uranyl ions and interfering ions are both 10 mg g^{-1}. 10 mg HSPI-O was dispersed into each flask, which was kept in a thermostatic shaker bath for 16 h at 298 K. After the adsorption, the equilibrium concentrations of uranyl ions and interfering ions were detected and the removal percentage of uranyl ions and interfering ions were calculated.

Simulated nuclear wastewater adsorption:

For investigating the adsorption performance in nuclear industry wastewater, simulated nuclear industry wastewater was configured according to the composition report of nuclear industry wastewater from a certain factory. The simulated nuclear wastewater containing uranyl ion and co-existing ions was prepared as followed: 0.254 g $MgCl_2·6H_2O$, 0.136 g $CaCl_2$, 0.046 g NaF, 0.148 g Na_2SO_4 and different mass of $UO_2(NO_3)_2·6H_2O$ were added into 1 L deionized

water. And various ions concentrations were recorded in Table S1. The adsorbent (10mg) was dispersed in 50 mL simulated nuclear industry wastewater, which was kept in a thermostatic shaker bath at 298 K for 16 h. The removal percentage of uranium was calculated.

S3 Radiation and temperature resistance studies

Radiation resistance:

The radiation resistance ability of HSPI-O was investigated in a GAMMATOR M-38-2 (USA) irradiator with a ^{60}Co source (γ-ray). 30 mg HSPI-O were exposed to γ-ray irradiation with dose of 1×10^5 Gy (dose rate: 6.2×10^3 Gy h^{-1}) at room temperature. The HSPI-O after radiation treatment was called as irra-HSPI-O. By comparing the FTIR spectra of the HSPI-O and irra-HSPI-O, we can judge whether HSPI-O was damaged.

Temperature resistance:

In view of the melting point and boiling point of water, the actual use temperature of the adsorbent can only range from 0 °C to 100 °C at most. In this study, the condition which was more severe than those in actual use was selected to explore the temperature resistance of the adsorbent. 30mg HSPI-O was heated at 120°C in an oven for 72 hours, and then frozen at -18°C for 72 hours after being taken out. The HSPI-O after high and low temperature treatment was called as temp-HSPI-O. By comparing the FTIR spectra of the HSPI-O and temp-HSPI-O, we can judge whether HSPI-O was damaged.

S4. Kinetics studies

The pseudo-first-order (PFO) and pseudo-second-order (PSO) models and intra-particle diffusion (IPD) models were analyzed by the following Eqs. (S1-S3):

$$\ln(q_e - q_t) = \ln q_e - k_1 t \tag{S1}$$

$$\frac{t}{q_t} = \frac{1}{k_2 q_e^2} + \frac{t}{q_e} \tag{S2}$$

$$q_t = k_3 t^{0.5} + C \tag{S3}$$

where q_e (mg g^{-1}) and q_t (mg g^{-1}) indicate the adsorption capacities of adsorbents at equilibrium and at time *t*, respectively; k_1 (h^{-1}) and k_2 (g mg^{-1} h^{-1}) represent the corresponding rate constants; k_3 (mg g^{-1} $h^{-0.5}$) represents the internal diffusion rate constant, *C* (mg g^{-1}) is a constant of material boundary layer and *t* (h) is the reaction time.

The relevant kinetics parameters were calculated from the slopes and intercepts of the plots of ln(q_e - q_t) versus t, t/q_t versus *t* and q_t versus $t^{0.5}$, which were shown in Table S3.

S5. Isotherm studies

For the adsorption isotherm studies, the linear forms of Langmuir and Freundlich isotherm models could be expressed as the following Eqs. (S4-S5):

$$\frac{C_e}{q_e} = \frac{1}{q_m K_L} + \frac{C_e}{q_m} \tag{S4}$$

$$\ln q_e = \ln K_F + \frac{1}{n} \ln C_e \tag{S5}$$

where C_e (mg L^{-1}) is the equilibrium concentration of uranium in the liquid phase, q_e (mg g^{-1}) is the adsorption capacity at equilibrium. q_m (mg g^{-1}) represents the maximum adsorption capacity and K_L (L mg^{-1}) is the adsorption equilibrium constant of the Langmuir model. K_F [(mg g^{-1})(L mg^{-1})$^{1/n}$] is the adsorption equilibrium constant of the Freundlich model and *n* is a constant.

The correlation coefficients and corresponding parameters, calculated from the slopes and intercepts of the plots of C_e/q_e versus C_e and $ln\ q_e$ versus $ln\ C_e$ were listed in Table S4.

S6. Thermodynamics studies

The change of thermodynamic parameters of sorption process was obtained using the following Eqs. (S6-S7):

$$\ln K_d = \frac{\Delta S}{R} - \frac{\Delta H}{RT} \tag{S6}$$

$$\Delta G = \Delta H - T\Delta S \tag{S7}$$

Where, ΔH, ΔS and ΔG represent the changes of enthalpy, entropy and Gibbs free energy in the adsorption process, which can illustrate the energy changes within absorbents, the degree of chaotic change during the adsorption process and whether the reaction is spontaneous process. *T* (K) and R are the Kelvin temperature and the gas constant, respectively. K_d is the distribution coefficient of uranium.

The values of ΔH and ΔS listed in Table S5 were derived from the slopes and intercepts of the plots of ln K_d versus T^{-1} (Fig. S4), and the values of ΔG were obtained using Eq. (S7).

S7. The elution efficiency (%) test

In order to choose a elution，elution efficiency (%) test of the uranium loaded HSPI-O adsorbent was performed using 50ml HNO_3 aqueous solutions with various concentrations (0.2 M, 0.15 M, 0.1M, 0.05M). Briefly, 10 mg HSPI-O was dispersed in 50ml 100 mg g^{-1} uranium solutions to reach adsorption equilibrium. After centrifugal separation, the adsorbent was dispersed in 50ml HNO_3 solutions of different concentrations to desorb at 25 ºC. The elution dfficiency (%) was calculated by the following Eqs. (S11):

$$Elution\ efficiency(\%) = \frac{C_{de}}{C_0 - C_e} \tag{S8}$$

where C_0 (mg L^{-1}) and C_e (mg L^{-1}) are the initial and equilibrium concentration of uranyl ion in the supernatant, C_{de} is the uranium concentration in the elution after desorption.

S8 Materials

3,3′,4,4′-Benzophenonetetracarboxylic dianhydride (BTDA), 2,6-diaminoanthraquinone (DAAQ), 1-methyl-2-pyrrolidone (NMP), hydroxylamine hydrochloride ($NH_2OH·HCl$), sodium carbonate (Na_2CO_3), sodium hydroxide (NaOH), nitric acid (HNO_3), uranyl nitrate hexahydrate ($UO_2(NO_3)_2·6H_2O$) were purchased from Aladdin Chemistry Co., Ltd. (China). The DAAQ and BTDA monomers were treated in a vacuum at 120 ℃ for 2 h before use. The solvent N-methylpyrrolidone (NMP) was distilled under reduced pressure. All other reagents were of AR grade and were used without further purification.

S9 Characterization

The morphology and chemical composition of HSPI and HSPI-O were characterized by scanning electron microscopy (SEM, INSPECTF, FEI, Netherlands) and energy dispersive X-ray spectroscopy (EDS). The functional groups of HSPI and HSPI-O were assessed by Perkin Elmer spectrometer (Model: Waltham, MA, USA) which was used from 4000 to 400 cm^{-1} to obtain the FT-IR spectra. N_2 adsorption and desorption isotherms were measured at the liquid nitrogen temperature using a Micromeritics ASAP 2010 instrument. The specific surface area and pore volume were calculated using the Brunauer-Emmett-Teller (BET) method. Residual concentrations of uranium and other metal elements were detected using Inductively Coupled Plasma-Mass Spectrometry (ICP-MS, Thermo Fisher, IRIS Intrepid II XSP).The crystalline structures of HSPI and HSPI-O were analyzed using an X-ray diffraction (XRD) system (Rigaku TTR III) equipped with Cu Ka radiation (λ = 1.54178 Å) at 40 kV and 150 mA. The compositions of HSPI and HSPI-O were analyzed by X-ray photoelectron spectroscopy (XPS) on Thermofisher Escalab Xi photoelectron spectrometer using Al Ka X-ray (hν=1486.6 eV) as the excitation source and a 500 μm light spot size. The radiation resistance abilitiy of HSPI-O were investigated in a GAMMATOR M-38-2 (USA) irradiator with a ^{60}Co source (γ-ray).

S10 Tables and Figures

Table S1 Composition of the simulated nuclear wastewater

Ion Species	Concentration (mg L^{-1})
Na^{+}	73.0
Ca^{2+}	49.0
Mg^{2+}	30.0
Cl^{-}	175.0
F^{-}	20.0
U^{6+}	0.2-1.0

Table S2 Binding energy and relative content of C 1s, O 1s and N 1s peaks for HSPI and HSPI-O analyzed by XPS.

Elements	HSPI		HSPI-O	
	Binding energy (eV)	Relative content (%)	Binding energy (eV)	Relative content (%)
C 1s	284.65	75.80	284.43	75.15
O 1s	531.41	18.36	531.22	18.54
N 1s	400.06	5.84	399.79	6.31

Table S3 Pseudo-first-order, pseudo-second-order and internal particle diffusion model constants and correlation coefficients (R^2) values of HSPI-O.

Pseudo-first-order model				Pseudo-second-order model				Internal particle diffusion model			
q_e^{exp} (mg g^{-1})	q_e^{cal} (mg g^{-1})	k_1 (h^{-1})	R^2	q_e^{exp} (mg g^{-1})	q_e^{cal} (mg g^{-1})	K_2 (g mg^{-1} h^{-1})	R^2	q_e^{cal} (mg g^{-1})	K_{id} (mg g^{-1} $h^{-0.5}$)	C	R^2
390	141	0.0312	0.3268	390	406	0.0033	0.9989	303	69.6	165	0.8432

Table S4 Isotherm constants and correlation coefficients (R^2) of HSPI-O.

Langmuir model				Freundlich model		
q_e^{exp} (mg g^{-1})	q_m (mg g^{-1})	K_L (L mg^{-1})	R^2	n	K_F [(mg g^{-1})(L mg^{-1})$^{1/n}$]	R^2
415	421	0.1833	0.9988	3.2530	93.49	0.9633

Table S5 The thermodynamic parameters of HSPI and HSPI-O for uranium adsorption.

Materials	ΔH (kJ mol^{-1})	ΔS (J mol^{-1} K^{-1})	ΔG (kJ mol^{-1})			
			298.15K	303.15K	308.15K	313.15K
HSPI	2.76	9.42	-0.05	-0.09	-0.14	-0.19
HSPI-O	-28.91	-80.32	-4.98	-4.57	-4.17	-3.77

Table S6 The elution efficiency of different concentrations of HNO_3

HNO_3 concentration (mol L^{-1})	Elution efficiency (%)
0.05	90.2
0.10	95.5
0.15	96.1
0.20	96.2

Table S7 Comparison of the uranium absorption capacity of HSPI-O with other powdery porous absorbents

Adsorbents	Experimental conditions				Adsorption capacity ($mg\ g^{-1}$)	Desorption time (min)	reference
	pH	T (K)	C_0 ($mg\ L^{-1}$)	m/V ($mg\ mL^{-1}$)			
NPS-GLCs	5.0	298	100	0.20	294.2	-	[S1]
Co-SLUG-35	9.0	298	100	1.00	85.0	240	[S2]
DSHM-DAMN	8.0	298	100	0.50	195.0	-	[S3]
AOGONRs	4.5	298	60	0.20	226.0	120	[S4]
GO–COOH/UiO-66	8.0	298	95	0.50	188.3	-	[S5]
MnO_2–Fe_3O_4–rGO	6.0	298	120	1.00	108.7	-	[S6]
PAM/GO	5.0	295	50	0.20	166.0	-	[S7]
UiO-66-NH_2	5.5	287	100	0.40	114.9	-	[S8]
MOF-76	3.0	298	140	0.40	298.0	-	[S9]
SZ-2	4.5	RT	75	0.20	58.0	-	[S10]
GO/MnO_2	4.0	298	45	0.25	66.8	1440	[S11]
Fe_3S_4	5.0	298	120	0.20	423.0	-	[S12]
HSPI-O	6.0	298	100	0.20	390.0	4	This work

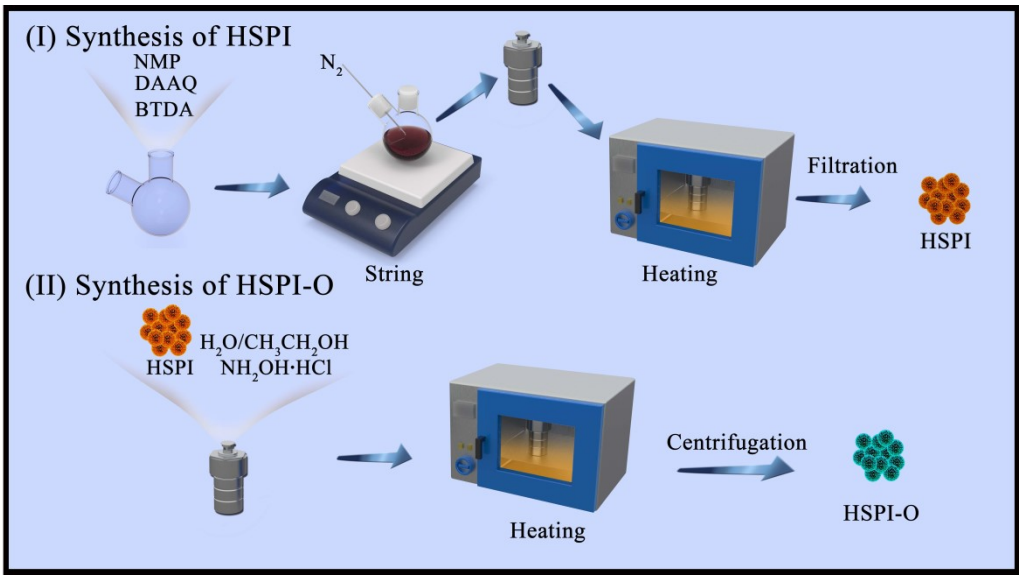

Scheme S1. Scheme of the fabrication procedures of HSPI and HSPI-O

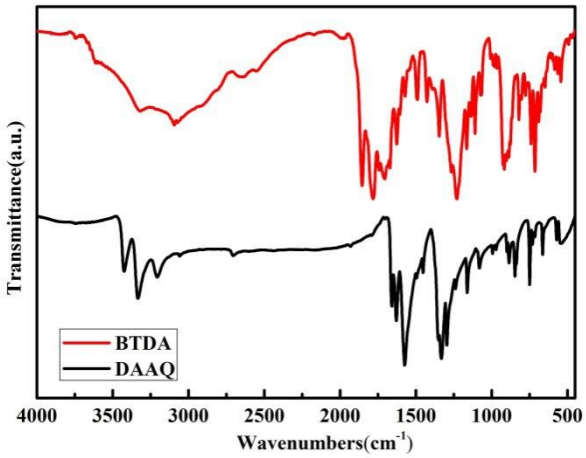

Figure S1. FTIR spectra of BTDA and DAAQ.

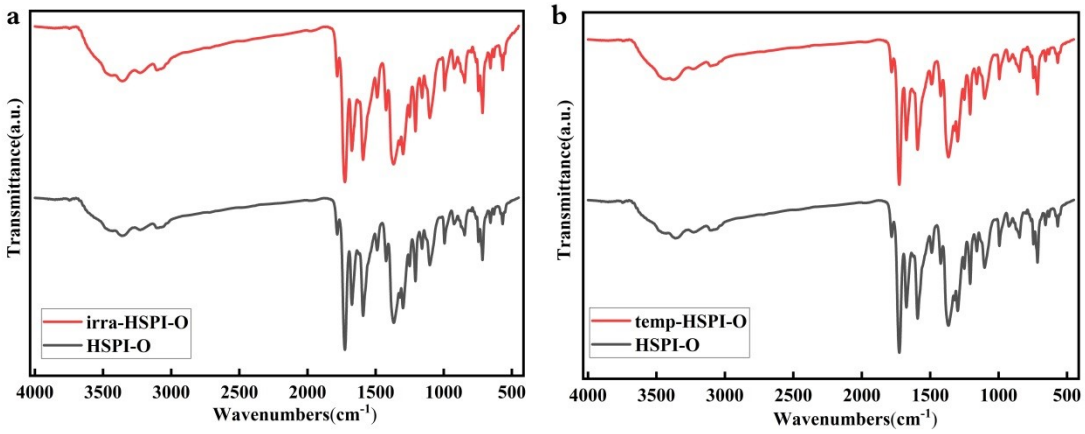

Figure S2. FTIR spectra of (a) HSPI-O and irra-HSPI-O, (b) HSPI-O and temp-HSPI-O.

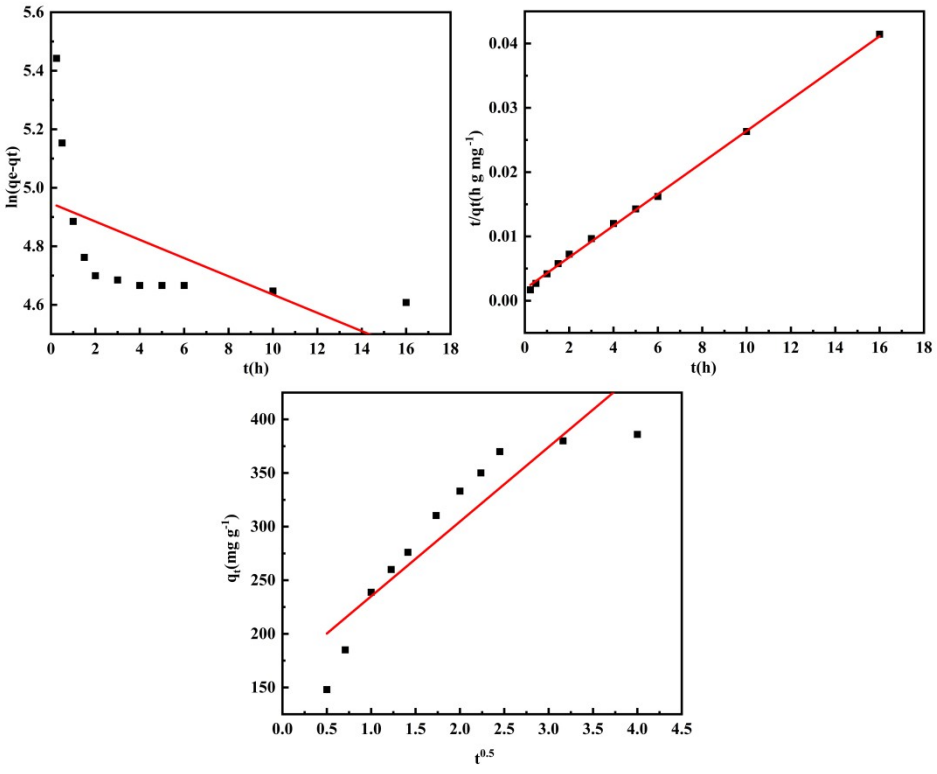

Figure S3. Fitting curves of adsorption kinetics of the HSPI-O (a) pseudo-first-order model, (b) pseudo-second-order model, (c)internal particle diffusion model.

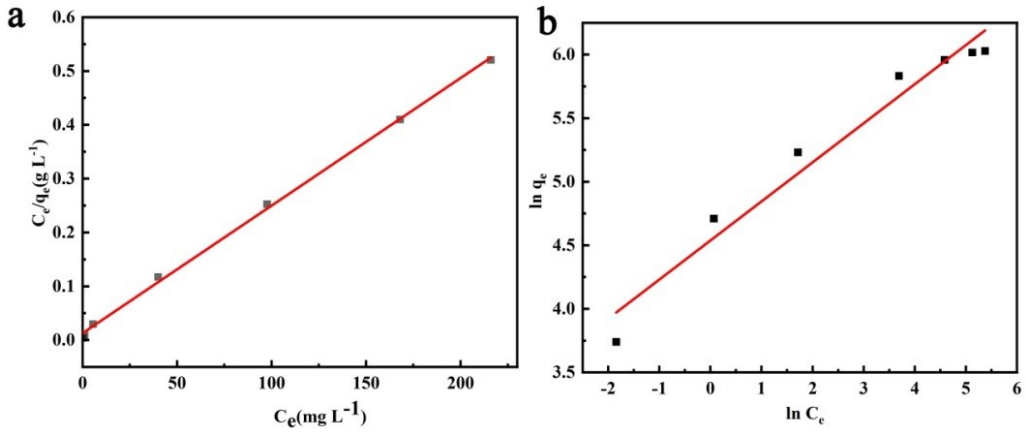

Figure S4. The isotherm models of HSPI-O (a) Langmuir model, (b) Freundlich model.

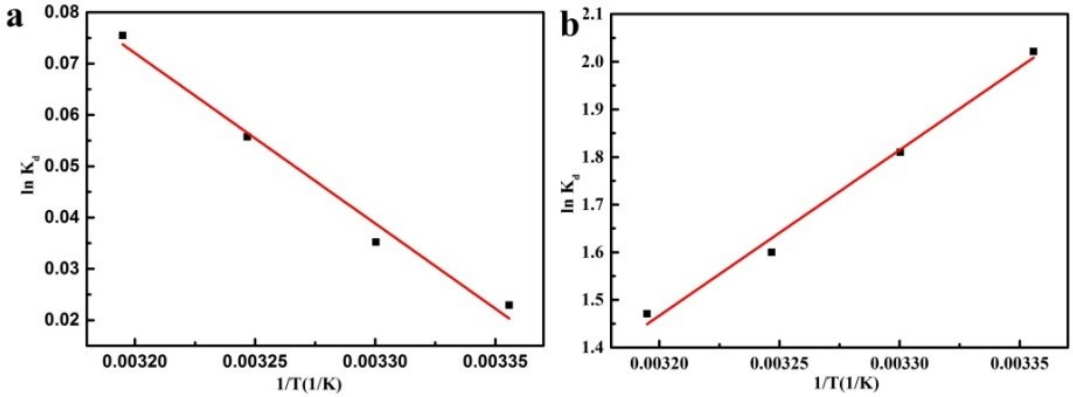

Figure S5. The relationship curves between lnK_d and 1/T (1/K). (a) HSPI, (b) HSPI-O.

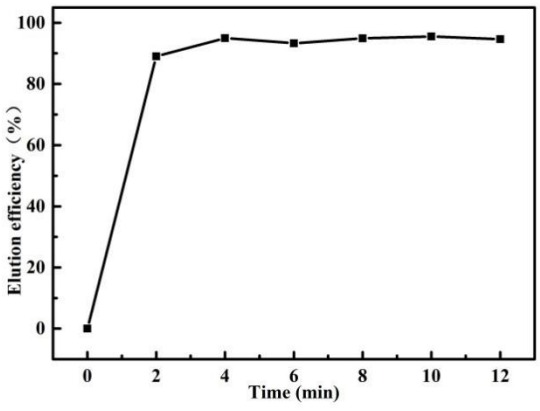

Figure S6. The influence of desorption time on the elution efficiency.

Reference

[S1].Z. Chen, W. Chen, D. Jia, Y. Liu, A. Zhang, T. Wen, J. Liu, Y. Ai, W. Song, X. Wang, N, P, and S Codoped Graphene-Like Carbon Nanosheets for Ultrafast Uranium (VI) Capture with High Capacity, Adv. Sci. 5 (2018) 1800235.

[S2].J.Q. Li, L.L. Gong, X.F. Feng, L. Zhang, H.Q. Wu, C.S. Yan, Y.Y. Xiong, H.Y. Gao, F. Luo, Direct extraction of U(VI) from alkaline solution and seawater via anion exchange by metal-organic framework, Chem. Eng. J. 316 (2017) 154-159.

[S3].J. Zhang, H. Zhang, Q. Liu, D. Song, R. Li, P. Liu, J. Wang, Diaminomaleonitrile functionalized double-shelled hollow MIL-101 (Cr) for selective removal of uranium from simulated seawater, Chem. Eng. J. 368 (2019) 951-958.

[S4].Y. Wang, Z. Wang, R. Ang, J. Yang, N. Liu, J. Liao, Y. Yang, J. Tang, Synthesis of amidoximated graphene oxide nanoribbons from unzipping of multiwalled carbon nanotubes for selective separation of uranium(vi), Rsc. Adv. 5 (2015) 89309-89318.

[S5].P. Yang, Q. Liu, J. Liu, H. Zhang, Z. Li, R. Li, L. Liu, J. Wang, Interfacial growth of a metal–organic framework (UiO-66) on functionalized graphene oxide (GO) as a suitable seawater adsorbent for extraction of uranium(vi), J. Mater. Chem. A 5 (2017) 17933-17942.

[S6].L. Tan, J. Wang, Q. Liu, Y. Sun, X. Jing, L. Liu, J. Liu, D. Song, The synthesis of a manganese dioxide–iron oxide–graphene magnetic nanocomposite for enhanced uranium(vi) removal, New J. Chem. 39 (2015) 868-876.

[S7].W. Song, X. Wang, Q. Wang, D. Shao, X. Wang, Plasma-induced grafting of polyacrylamide on graphene oxide nanosheets for simultaneous removal of radionuclides, Phys. Chem. Chem. Phys. 17 (2015) 398-406.

[S8].B.C. Luo, L.Y. Yuan, Z.F. Chai, W.Q. Shi, Q. Tang, U(VI) capture from aqueous solution by highly porous and stable MOFs: UiO-66 and its amine derivative, J. Radioanal. Nucl. Chem. 307 (2015) 269-276.

[S9].W. Yang, Z.Q. Bai, W.Q. Shi, L.Y. Yuan, T. Tian, Z.F. Chai, H. Wang, Z.M. Sun, MOF-76: from a luminescent probe to highly efficient U(VI) sorption material, Chem Commun (Camb) 49 (2013) 10415-10417.

[S10]. T. Zheng, Z. Yang, D. Gui, Z. Liu, X. Wang, X. Dai, S. Liu, L. Zhang, Y. Gao, L. Chen, D. Sheng, Y. Wang, J. Diwu, J. Wang, R. Zhou, Z. Chai, T.E. Albrecht-Schmitt, S. Wang, Overcoming the crystallization and designability issues in the ultrastable zirconium phosphonate framework system, Nat Commun 8 (2017) 15369.

[S11]. N. Pan, L. Li, J. Ding, S. Li, R. Wang, Y. Jin, X. Wang, C. Xia, Preparation of graphene oxide-manganese dioxide for highly efficient adsorption and separation of Th(IV)/U(VI), J. Hazard. Mater. 309 (2016) 107-115.

[S12] S.Y. Yang, Q. Li, L. Chen, Z.S. Chen, B.W. Hu, H.H. Wang, X.K. Wang, Synergistic removal and reduction of U(VI) and Cr(VI) by Fe3S4 micro-crystal, Chem. Eng. J. 385 (2020) 123909.